Journal of Sustainable Mining 17 (2018) 20–33

HOSTED BY

Contents lists available at ScienceDirect

Journal of Sustainable Mining

journal homepage: http://www.elsevier.com/locate/jsm

Research paper

Studying the effect of some parameters on the stability of shallow tunnels

Wael R. Abdellah [a, *], Mahrous A. Ali [b], Hyung-Sik Yang [c]

[a] Mining and Metallurgical Engineering Dept., Faculty of Engineering, University of Assiut, Assiut, 71516, Egypt
[b] Mining and Petroleum Engineering Dept., Faculty of Engineering, University of Al-Azhar, Qena, Egypt
[c] Energy and Resource Engineering Dept., College of Engineering, Chonnam National University, South Korea

ARTICLE INFO

Article history:
Received 19 November 2017
Received in revised form
10 January 2018
Accepted 1 February 2018
Available online 13 February 2018

Keywords:
Tunnel shape
Rock joints
Numerical modelling
Stability indicators

ABSTRACT

Several factors have crucial impact on the serviceability of underground openings including: the quality of rock mass; the presence of rock joints and their geometrical properties; the state of in-situ stress ratio; the depth below surface and opening geometry. This paper only investigates the effect of two parameters on the stability of underground shallow tunnels, namely: the presence of rock joints in the rock mass matrix and the shape of the excavation. A series of two-dimensional elasto-plastic finite-element models has been constructed using rock-soil, RS^{2D}, software. Consequently, parametric stability analysis has been conducted for three different tunnel shapes (e.g. circular, square and horseshoe) with/without joint inclusion. Four reference points have been assigned in the tunnel perimeter (e.g. back, sidewalls and floor) to monitor the state of stress-displacement in the rock mass around them. The results indicate that the weak performance of a tunnel opening occurs with a square-shaped opening and when joints exist in the rock mass. In addition, the normal stress along joints sharply drops in the vicinity of a tunnel opening. Moreover, the direction of shear stress is reversed. Thus, it causes inward shear displacement.

1. Introduction

Tunnels are constructed to serve several purposes (e.g. irrigation, sanitary drainage, conveyance, and hydro-electrical power stations) in geotechnical, civil and mining engineering. They have become an essential component of modern societies particularly in big cities (Madkour, 2012; Elshamy, Attia, Fawzy, & Abdel Hafez, 2013; Panjia, Koohsari, Adampira, Alielahi, & Marnani, 2016). Therefore, their performance during their service/entire life is of major concern. This performance is primarily influenced by the characteristics of rock mass (e.g. strength, quality) and the state of in-situ stresses. The failure mechanism of rock mass is mainly ruled by the behaviour of discontinuities (e.g. faults, joints, bedding planes, shear zones, dykes, etc.). In rock mechanics, joints usually refer to any type of discontinuities (Ghorbani, Zahedi, & Asaadi, 2015; Kulatilake, Qiong, Zhengxing, & Fuxing, 2013; Piyal & Konietzky, 2016).

Rock joints are regularly spaced and usually occur in a parallel set of joint networks. However, sometimes they may exist at various dip directions. Therefore, rock mass is broken up into a blocky structure (Jia & Tang, 2008). In-situ stress ratio has a significant effect on the stability of underground tunnels (particularly at great depths). Therefore, in high stress environments the stability of tunnels is controlled by the induced-stresses and joints that grow parallel to the tunnel boundary (Martin, Kaiser, & McCreath, 1999; Raju, 2013).

The construction of tunnels in a terrain with mixed lithology (e.g. incompetent, quasi-elastic with faults, folds, weak, fragile rocks, presence of a considerable amount of clay minerals, etc.) and varied ground conditions (e.g. tectonically active, thrusts of different magnitudes or a trapped water reservoir) is a big challenge for engineers particularly at great depths with high overburden pressures. Consequently, several problems are encountered in the supporting of tunnels, due to squeezing, swelling, water existence, poor rock state, and excessive temperatures and gases in rocks. Tunnel squeezing is a result of the plastic behaviour of rock mass under high overburden stresses, particularly when a considerable amount of clay/micaceous minerals are presented and there is low swelling capacity. Therefore, to optimize the costs of a support system and avoid instability problems, the tunnel which experiences squeezing conditions must be allowed to deform. Such

* Corresponding author.
E-mail address: wre544@gmail.com (W.R. Abdellah).

https://doi.org/10.1016/j.jsm.2018.02.001

deformation has to be considered when planning the size of an excavation. Experience with different support systems (e.g. steel ribs, compressible backfill, and shotcrete) in such terrain reveals that empirical methods do not provide reliable evaluation of the design parameters (Jethwa, Dube, Singh, & Singh, 1984; Saini, Dube, & Singh, 1989).

Different tools can be employed to assess the stability of underground tunnels, such as: analytical, empirical and numerical modelling methods. The analytical methods comprise of equations which are used to estimate the stresses and deformation around simple openings (e.g. circular openings). They are primarily developed by Kirsch (1898), Ladanyi (1974), Brady (1977), Brady and Lorig (1988). However, these methods cannot provide adequate solutions for complex geometries.

The empirical methods (e.g. stability graph method) are based on past experiences, reported case studies and rock mass classification systems. Such methods use the geomechanical properties of rock mass to provide an estimate for the rock design support system. However, these methods do not account for all factors influencing the stability of underground openings. Therefore, they are widely replaced by numerical modelling methods. Numerical methods are reliable, robust and efficient at providing a complete solution and can handle very complex geometries. They can also be adopted ahead of time, before actual excavation, to select the optimum design/sequence (Berisavljević, Dušan, Čebašek, & Rakić, 2015; Maleki, Mahyar, & Meshkabadi, 2011; Soren, Budi, & Sen, 2014). Numerical modelling analyses have been conducted by many researchers to investigate the effects of rock joints on the performance of underground tunnels. A basic scale-model has been developed by Barton (1972) to examine the performance of rock support installed into jointed rock mass. The behaviour of rock mass deformation around the tunnel has been analysed by Goodman, Heuze, and Bureau (1972). The impact of a fault on the tunnel has been investigated by Jeon, Kim, Seo, and Hong (2004).

A sensitivity analysis was carried out by Yeung and Leong (1997) using discontinuous deformation analysis (DDA) to study the effect of the attribute of joints in a rock mass matrix. Two-dimensional discrete element code (UDEC) was employed by Hao and Azzam (2005) to examine the effect of some fault parameters on the stability of a tunnel. The geometrical properties of rock joints (orientation, dimensions) have been studied by Jiang, Tanabashi, Li and Xiao (2006). The stability of underground openings in blocky rock mass has been investigated by Goodman and Shi (1985). Although many researchers have investigated analytically and experimentally the impacts of stress state and rock joints on the stability of underground openings, rock failure mechanism of underground openings under complex geological conditions is not fully explained in the literature. Eberhardt (2001) examined the impact of rock joints and stress regime on tunnel behaviour, due to stress rotation ahead of the tunnel, using three-dimensional analysis. This paper aims to evaluate the impact of different tunnel shapes and presence of rock joints on the performance of underground shallow tunnels in terms of the state of stress-displacement. The following section briefly discusses various stability indicators used in this parametric stability analysis to assess the serviceability of a tunnel opening.

2. Stability indicators

A range of failure evaluation criteria could be adopted to assess the stability of underground openings. In this study, the state of stress-displacement around a tunnel opening is monitored and introduced in terms of induced-stress, stress concentration, strength of rock mass, convergence ratio of tunnel shoulders, ratio of roof sag and floor heave, and the depth of yielding zones into the rock mass surrounding tunnel opening. The following subsection briefly presents these evaluation criteria.

2.1. Induced-stress

Eq. (1) represents the induced-stress as the difference between pre- and post-excavated stress, as per Eq. (1).

$$\text{Induced} - \text{stress} = \sigma_1 - \sigma^0 \tag{1}$$

where:

σ_1 – stress results after excavating the tunnel, and
σ^0 – in-situ stress (virgin stress).

2.2. Stress concentration

Stress concentration regions around tunnel opening are measured using the stress concentration factor, *SCF*. As shown in Eq. (2), *SCF* is defined as the ratio of post-excavated stress, σ_1 to pre-excavated stress, σ^0 (Zhang & Mitri, 2008).

$$SCF = \frac{\sigma_1}{\sigma^0} \tag{2}$$

2.3. Rock mass strength

The strength of rock mass, after excavating a tunnel opening, is monitored using strength factor (*SF*). This factor is analogous to the factor of safety which may have several formulations based on different assumptions (Sheorey, 1997) In Eq. (3), the *SF* is defined as the ratio of unconfined compressive strength of intact rock (*UCS*) to post-excavated stress (σ_1). Thus, the serviceability of a tunnel opening will be considered unsatisfactory if $SF < 1.0$.

$$SF = \frac{UCS}{\sigma_1} \tag{3}$$

2.4. Potential stress failure (PSF)

Another factor called potential stress failure (*PSF*) can be used to assess the stability of underground tunnels, as shown in Eq. (4). The, *PSF* is calculated at the boundary of the tunnel, where minor principal stress (σ_3) vanishes (Mitri, 2007).

$$PSF = \frac{\sigma_1}{UCS_{rm}} \times 100 \tag{4}$$

where:

σ_1 – maximum computed boundary stress due to excavation, and
UCS_{rm} – uniaxial compressive strength of rock mass and is estimated as per Eq. (5).

$$UCS_{rm} = UCS\ \sqrt{s} \tag{5}$$

where:
s – Hoek-Brown constant, $\sqrt{s} \geq 0.50$, and
UCS – lab uniaxial compressive strength of intact rock.
PSF is only adopted when the Hoek-Brown failure criterion is employed (e.g. elasto-plastic brittle shear failure analysis)

Table 1
Geomechanical properties of rock mass used in this analysis.

property	Limestone	Slate
γ, MN/m^3	0.026	0.025
UCS, MPa	30–250	100–200
υ	0.30	0.25
σ_t, MPa	0.60	0.10
∅, deg.	40	35
E, GPa	35	2.60
C, MPa	1	0.25
Ψ, deg.	20	15

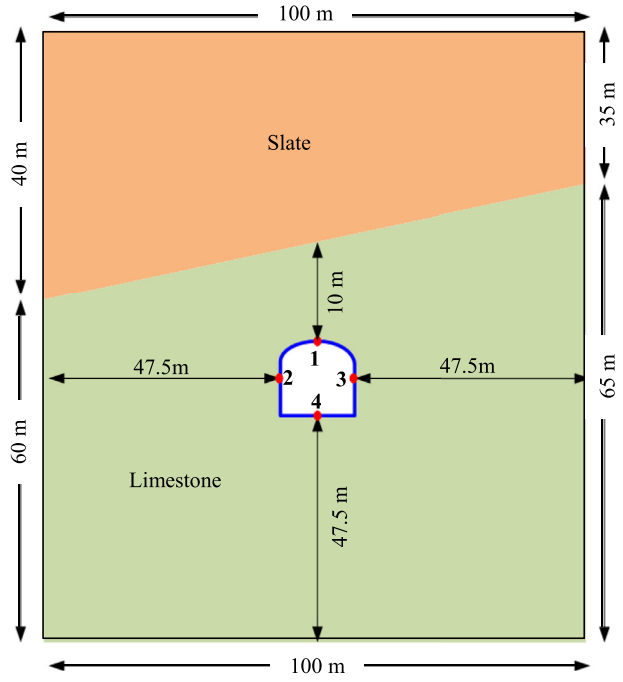

Fig. 1. Geometry and dimensions of a horseshoe tunnel without including rock joints (Reference model).

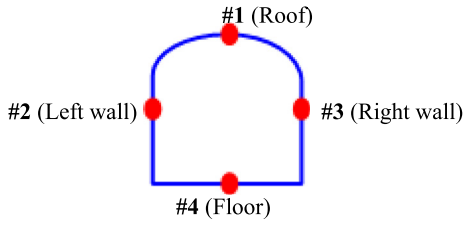

Fig. 2. Four reference points assigned in the perimeter of the tunnel.

(Abdellah, Mitri, Thibodeau, & Moreau-Verlaan, 2012). Therefore, it won't be considered in this analysis.

2.5. Wall convergence ratio (WCR)

The magnitude of wall closure to the tunnel horizontal span is known as wall convergence (*WCR*), as shown in Eq. (6) (Abdellah, 2015; Zhang & Mitri, 2008).

$$WCR = \left(\frac{W_\circ - W_1}{W_\circ}\right) \times 100 \tag{6}$$

where:

$W_\circ$ – original span or width of a tunnel opening, and
W_1 – width of the tunnel opening after deformation.

For the purpose of this study, the instability condition of the tunnel occurs when the ratio of the wall convergence exceeds 2% (e.g. $WCR > 2.0\%$) from the width of the opening.

2.6. Roof sag ratio (RSR)

As shown in Eq. (7), the roof sag ratio is defined as the ratio of crown (roof) sag to the original vertical span (height) of the opening as (Zhang & Mitri, 2008).

$$RSR = \left(\frac{\Delta_S}{H}\right) \times 100 \tag{7}$$

where:

Δ_S – roof sag, and
H – original height or vertical span of the tunnel.

In this analysis, it is assumed that a tunnel's unsatisfactory performance is reached when the sag ratio in the tunnel back/roof exceeds 1% of the height of the opening (e.g. $RSR > 1.0\%$).

2.7. Floor heave ratio (FHR)

Floor heave ratio (*FHR*) is shown in Eq. (8). It is defined as the ratio of floor heave, Δ_y to the original height (e.g. vertical span, *H*) of the tunnel.

$$FHR = \left(\frac{\Delta_y}{H}\right) \times 100 \tag{8}$$

where:

Δ_y – floor heave

In this sensitivity analysis, the stability of a tunnel opening is considered unsatisfactory if the ratio of the floor heave goes beyond 0.5% (e.g. $FHR > 0.50\%$) of the vertical span of the opening.

2.8. Extent of yielding zones

Yielding is a common built-in function in most numerical modelling tools when elasto-plasticity is adopted. The rock mass is yielded when it is loaded beyond its elastic limit. In this investigation, the Mohr-Coulomb yielding function is employed with elastic-perfectly plastic analysis. This function is used to measure the extent of failure zones in the rock mass around the tunnel boundary.

Table 2
In-situ stress values at tunnel depth of 50 m below surface.

Principal stress	Magnitude, MPa	Orientation	Average unit weight, $\gamma_{ave.}$ MN/m^3	Depth, Z, m	Stress ratio, $K = \frac{\sigma_h}{\sigma_v} = 1 + \frac{8}{\sqrt{Z}}$ (Zhang & Mitri, 2008)
$\sigma_1 = \sigma_h = K \times \sigma_v$	2.72	East-West	0.0255	50	2.13
$\sigma_3 = \sigma_v = \gamma_{ave.} \times Z$	1.28	Vertical			

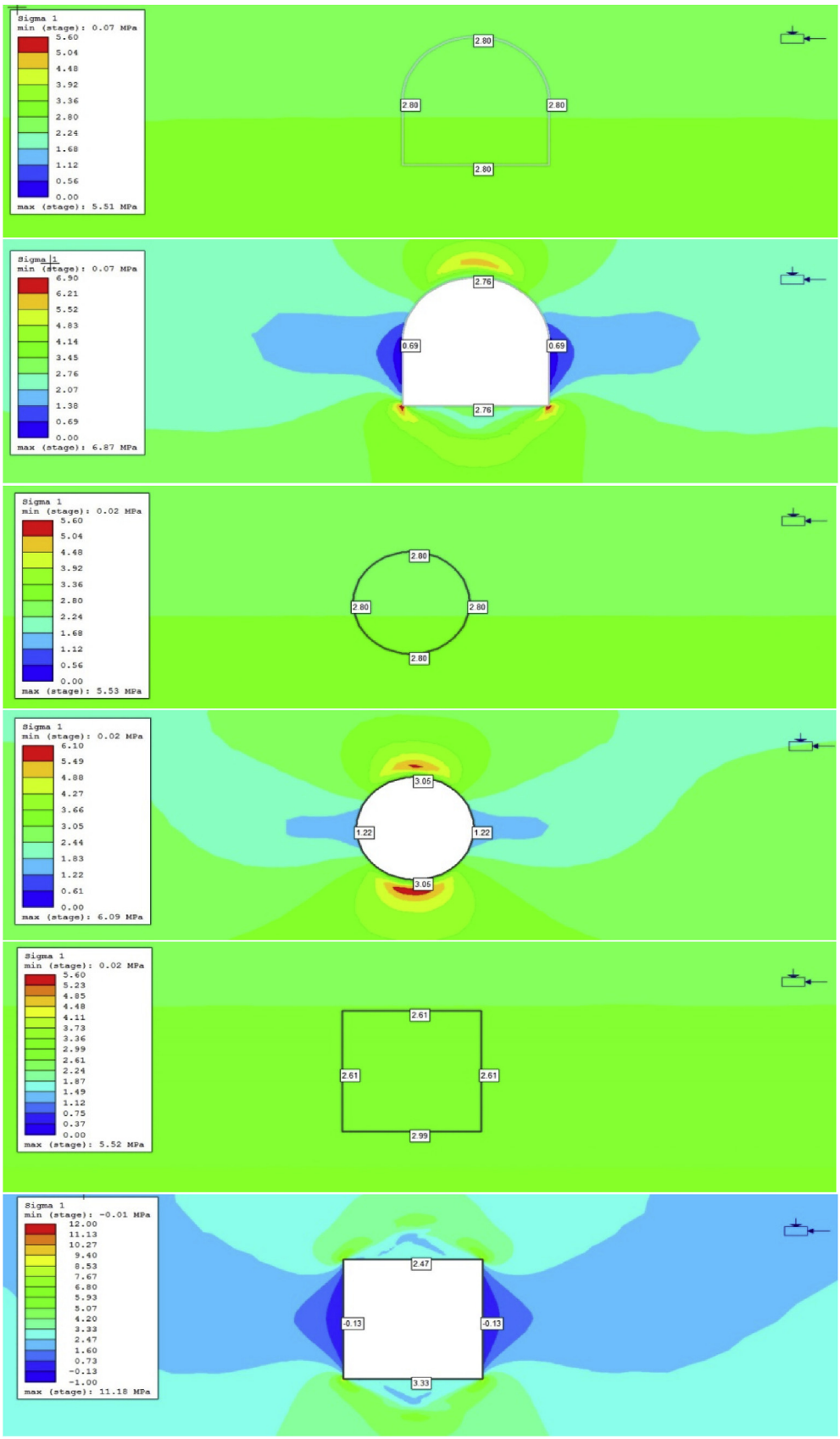

Fig. 3. Contours of pre-and post-excavating stresses around the boundary of various tunnel shapes.

Table 3
State of stresses around the boundary of different tunnel shapes before and after-excavating.

Tunnel shape	Pre-excavating stress,σ_0 MPa				Post-excavating stress,σ_1 MPa				Induced-stress, MPa ($\sigma_1 - \sigma_0$)			
	Roof (#1)	Left wall (#2)	Right wall (#3)	Floo (#4)	Roof (#1)	Left wall (#2)	Right wall (#3)	Floor (#4)	Roof (#1)	Left wall (#2)	Right wall (#3)	Floor (#4)
Circular	2.80	2.80	2.80	2.80	3.05	1.22	1.22	3.05	0.25	−1.58	−1.58	0.25
Horseshoe	2.80	2.80	2.80	2.80	2.76	0.69	0.69	2.76	−0.04	−2.11	−2.11	−0.04
Square	2.61	2.61	2.61	2.99	2.47	−0.13	−0.13	3.33	−0.14	−2.88	−2.88	0.34

The unsatisfactory condition is met if the length of the yielding zones in the rock mass exceeds the anchorage length of the primary rock support. This length is determined according to the principle whereby the resin grouted rebar can sustain 1-ton of axial load per 1-inch anchorage length. Therefore, the primary rock support of 12-ton tensile capacity requires 12-inch (approximately 30 cm) anchorage length. Alternatively, the 12-inch anchorage length is termed as critical anchorage length over which full capacity is developed. For the purpose of this study, it is assumed that the resin grouted rebar installed in the tunnel's roof, walls and floor, which is 1.8 m-long, requires at least 30 cm of resin anchorage in order to achieve full-design strength. Therefore, tunnel unsatisfactory performance is reached when the depth of the failure zones exceeds 1.5 m (anchorage length $<$ 30 cm).

3. Problem definition and modelling set up

In this study, numerical modelling analysis was carried-out using a two-dimensional elasto-plastic finite-element code (e.g. Rock-Soil, RS^{2D}); with the Mohr-Coulomb yield-based function. The geomechanical properties of the rock mass used in this analysis are listed in Table 1. A reference model, where a horseshoe tunnel is located at a depth of 50 m below the surface with dimensions of 5 × 5-ms, is created as depicted in Fig. 1.

In this analysis, four key/reference points were assigned in the tunnel's perimeter, as shown in Fig. 2, to monitor the state of stress-displacement around them. A series of two-dimensional elasto-plastic finite-element models were constructed using rock-soil, RS^{2D}, software. In this analysis, tunnel shape and the presence of rock joints were considered in order to examine their impact on the performance of an underground tunnel opening. The pre-existing stresses (e.g. in-situ stresses) applied in this modelling analysis are calculated and listed in Table 2.

4. Results and discussion

Excavating underground openings undoubtedly violates the equilibrium state of pre-existing initial stresses in the rock mass. Therefore, rock mass tends to readjust its behaviour until a new equilibrium state is attained. Otherwise, collapse may result due to high stress concentration in some regions. The results of this parametric stability analysis are presented and discussed for different tunnel shapes in terms of the state of stress-displacement (e.g. major induced-stress, *SCF* and *SF*, *WCR*, *RSR*, *FHR* and the spread of yielding zones in the rock mass) with/without the presence of rock joints.

4.1. Case I – no joints are present

In this subsection, only the effect of tunnel shapes (i.e. without including rock joints) on the performance of tunnel behaviour will be presented and discussed in terms of the state of stress-displacement and extent of yielding zones in the rock mass surrounding a tunnel opening.

4.1.1. Induced-stress

The pre- and post-excavating stresses around a tunnel's boundary, in various tunnel shapes, are shown in Fig. 3 and listed in Table 3. The induced-stresses are then calculated according to Eq. (1) and plotted as shown in Fig. 4. It is noticeable that the stress distribution is completely changed after excavating the tunnel. For instance, high compressive stresses are concentrated around the roof and the floor of a circular tunnel and the floor of a square tunnel. However, low (i.e. tensile) stresses are concentrated around the sidewalls of a circular tunnel, as well as the roof, the floor and the sidewalls of a horseshoe tunnel and the roof and the sidewalls of a square tunnel.

4.1.2. Deformation/convergence

In this section, the deformation of rock mass around the boundary of different tunnel shapes is presented and discussed in

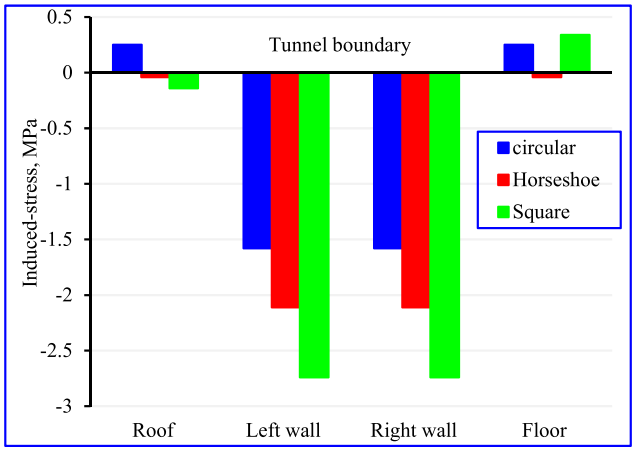

Fig. 4. Estimated induced-stresses around the boundary of different tunnel shapes.

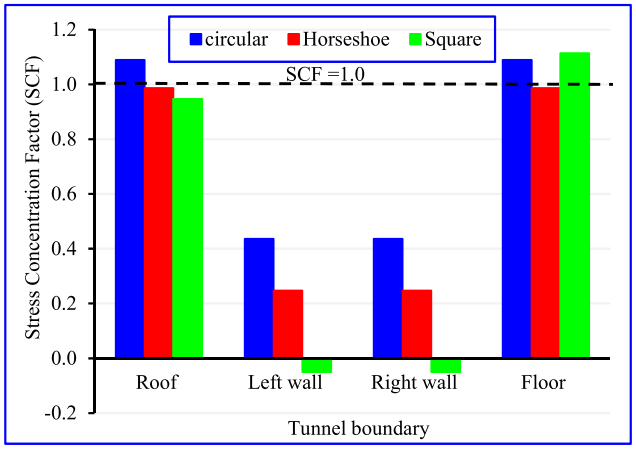

Fig. 5. Stress concentration around the boundary of different tunnel shapes.

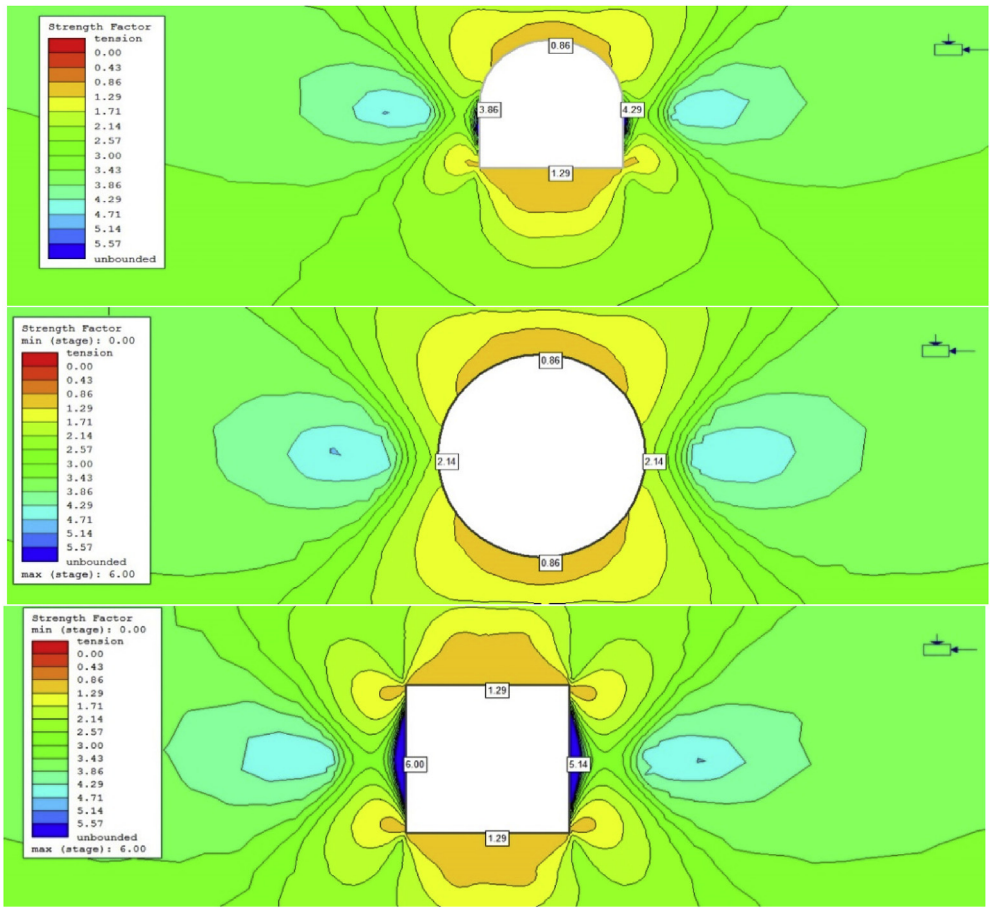

Fig. 6. Rock mass strength contours around different shapes of tunnel openings after they have been created.

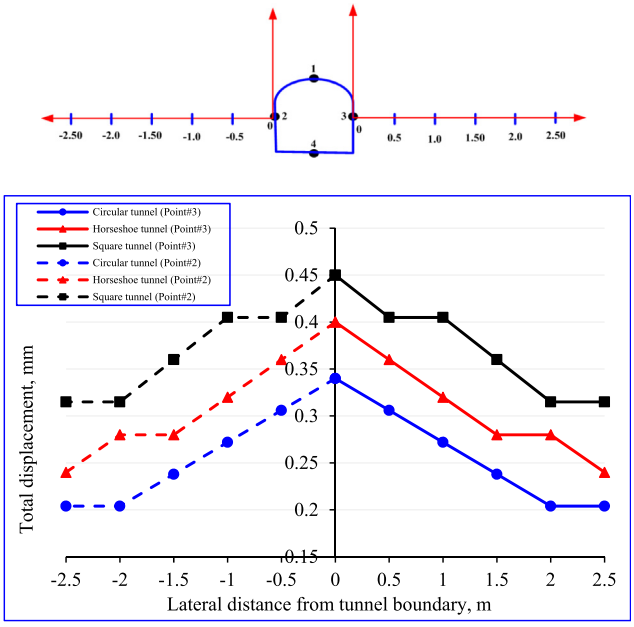

Fig. 7. Total displacements around a tunnel's sidewalls (measured at lateral distances from the reference points #2 & #3) for different tunnel shapes.

terms of total displacement, walls' convergence ratio (*WCR*), roof sag ratio (*RSR*) and floor heave ratio (*FHR*).

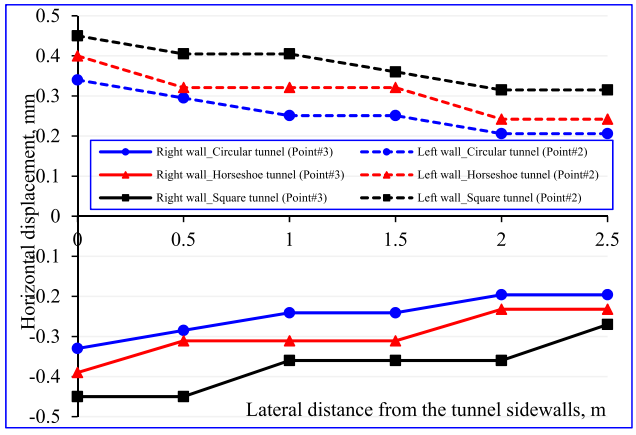

Fig. 8. Horizontal displacements around a tunnel's sidewalls (measured at lateral distances from the reference points #2 & #3) for different tunnel shapes.

4.1.2.1. Total displacement. Fig. 7 shows the total displacements around the boundary of different tunnel shapes, measured at various horizontal distances from the key points (e.g. #2 & #3) located in the perimeter of the tunnel's sidewalls.

Fig. 7 shows that the maximum total displacements of rock mass occur in the perimeters (i.e. at zero meters from the boundary) of the tunnel. For instance, the maximum total displacements which are monitored and reported on the boundary of square, horseshoe and circular tunnels are 0.45 mm, 0.40 mm and 0.34 mm

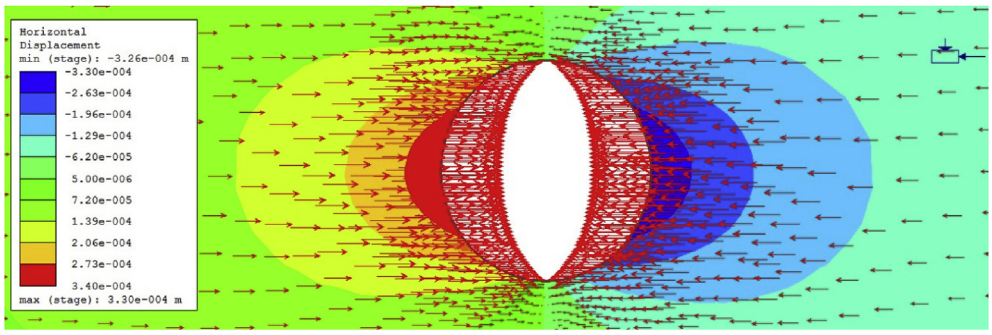

Fig. 9. Vectors indicate the direction of the horizontal displacements in circular tunnel's sidewalls.

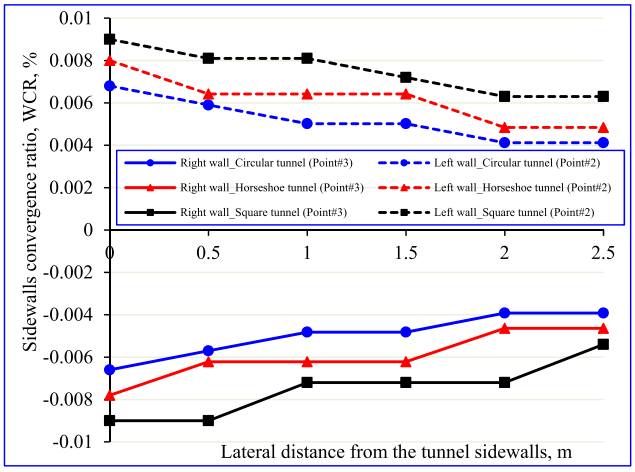

Fig. 10. The convergence ratio of a tunnel's sidewalls for different tunnel shapes at various lateral displacements measured from the sidewalls' key points (#2 & #3).

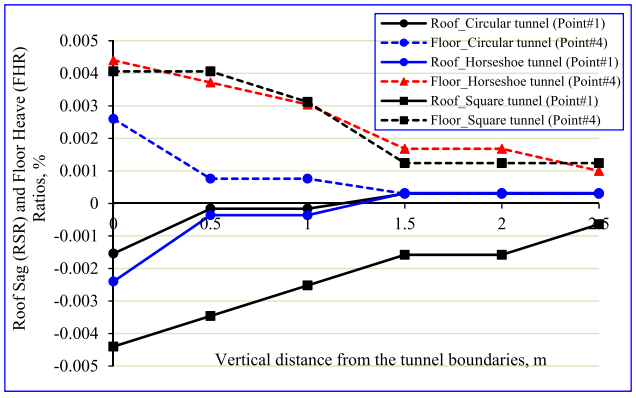

Fig. 12. Roof sag and floor heave ratio estimated around the key points (#1 & #4) at various vertical distances from the tunnel boundary.

respectively. In addition, these displacements decrease as the lateral distance from the tunnel boundary increases.

4.1.2.2. Horizontal displacement. The horizontal displacements of rock mass around the sidewalls of a tunnel opening are depicted in Fig. 8. It can be shown that the left and right walls tend to move towards the entire of the tunnel. Alternatively, key point #2 (located on the left wall of the tunnel boundary) moves to the right direction and thus yields a positive displacement. On the other hand, key point #3 (situated on the right wall of the tunnel boundary) moves to the left direction thus providing negative displacement, after a tunnel opening has been introduced, as shown in Fig. 9.

The convergence ratio of the tunnel's sidewalls is estimated using Eq. (6) and depicted as shown in Fig. 10. It can be shown that the maximum convergence ratio occurs in the sidewalls of a square tunnel (i.e. ∓0.009%). However, these ratios are very distant from the chosen threshold value ($WCR > 2\%$). Thus, the performance of all tunnels is satisfactory.

4.1.2.3. Vertical displacement. Fig. 11 depicts rock mass vertical displacements around the roof and the floor of a tunnel opening.

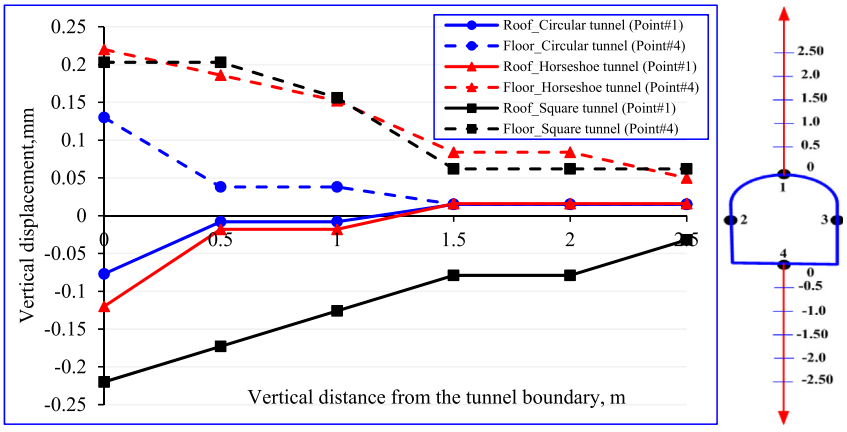

Fig. 11. Rock mass vertical displacements around a tunnel's roof and floor for different tunnel shapes and various vertical displacements measured from key points #1 and #4.

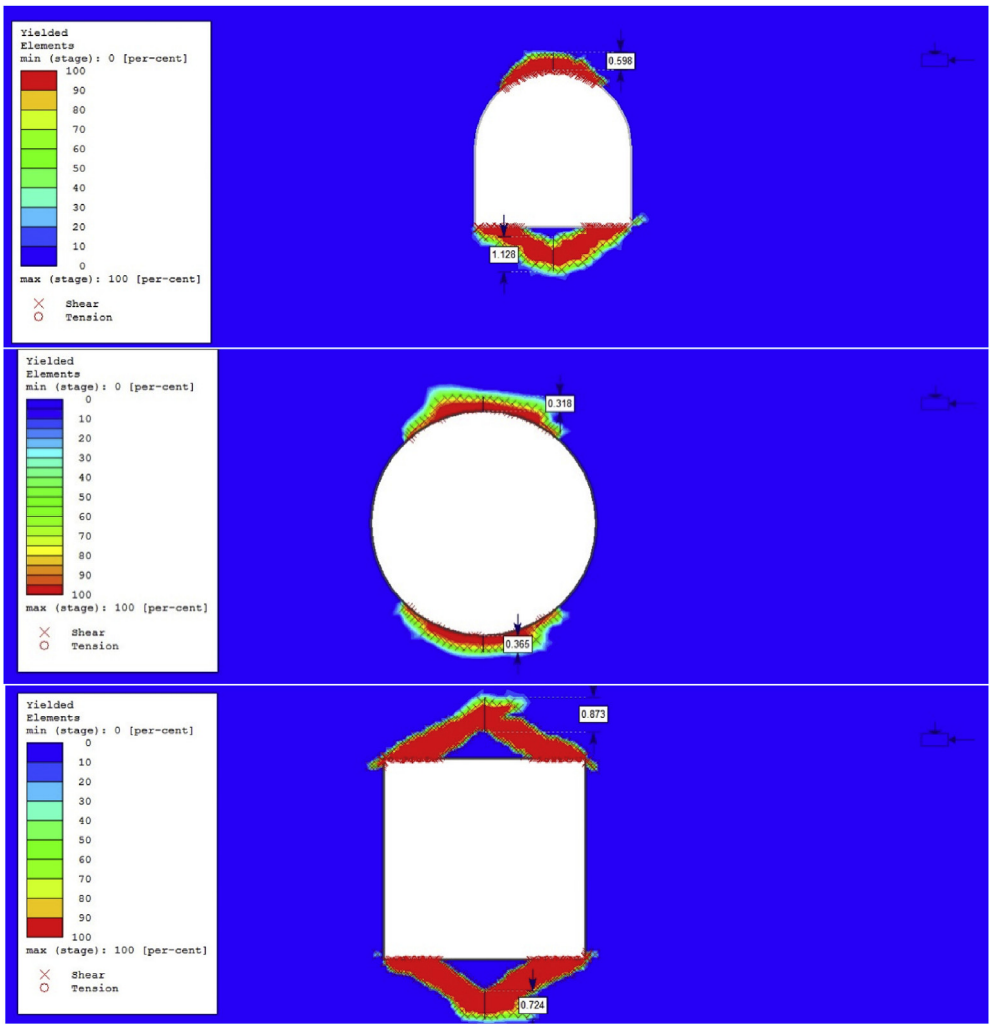

Fig. 13. Extent of yielding zones in the rock mass around different tunnel shapes.

Table 4
Geomechanical properties of joints.

Normal stiffness, K_n	21 GPa
Shear stiffness, K_s	15 GPa
Friction angle, ⌀ (deg.)	39°

Such displacements are measured at various distances from key points #1 and #4. It can be shown that maximum rock mass vertical displacements which occur in the roof and floor of a square tunnel are −0.22 mm and +0.203 mm respectively. Whilst, the maximum rock mass vertical displacement occurs in the floor of a horseshoe tunnel and equals +0.22 mm.

4.1.2.4. Roof sag and floor heave ratio. The roof sag and floor heave ratio have been estimated using Eq. (7) and Eq. (8) respectively. Fig. 12 displays the sag ratio of a tunnel's roof and the heave ratio of a tunnel's floor for different tunnel shapes at various vertical distances measured from key points #1 and #4. It can be shown that the ratio of roof sag and floor heave is insignificant. For instance, the maximum roof sag (*RSR*) which occurs in a square tunnel is −0.0044%. Whereas, the maximum heave (*FHR*) which occurs in horseshoe and square tunnels is +0.0044% and +0.00406%, respectively. Thus, the performance of all of the tunnels is still satisfactory as *RSR* and *FHR* < 1%.

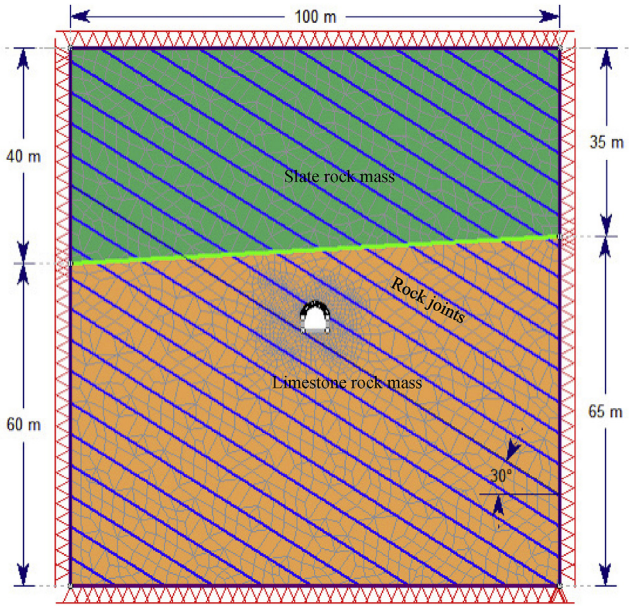

Fig. 14. Joint model, boundary conditions and the geometry of a horseshoe tunnel.

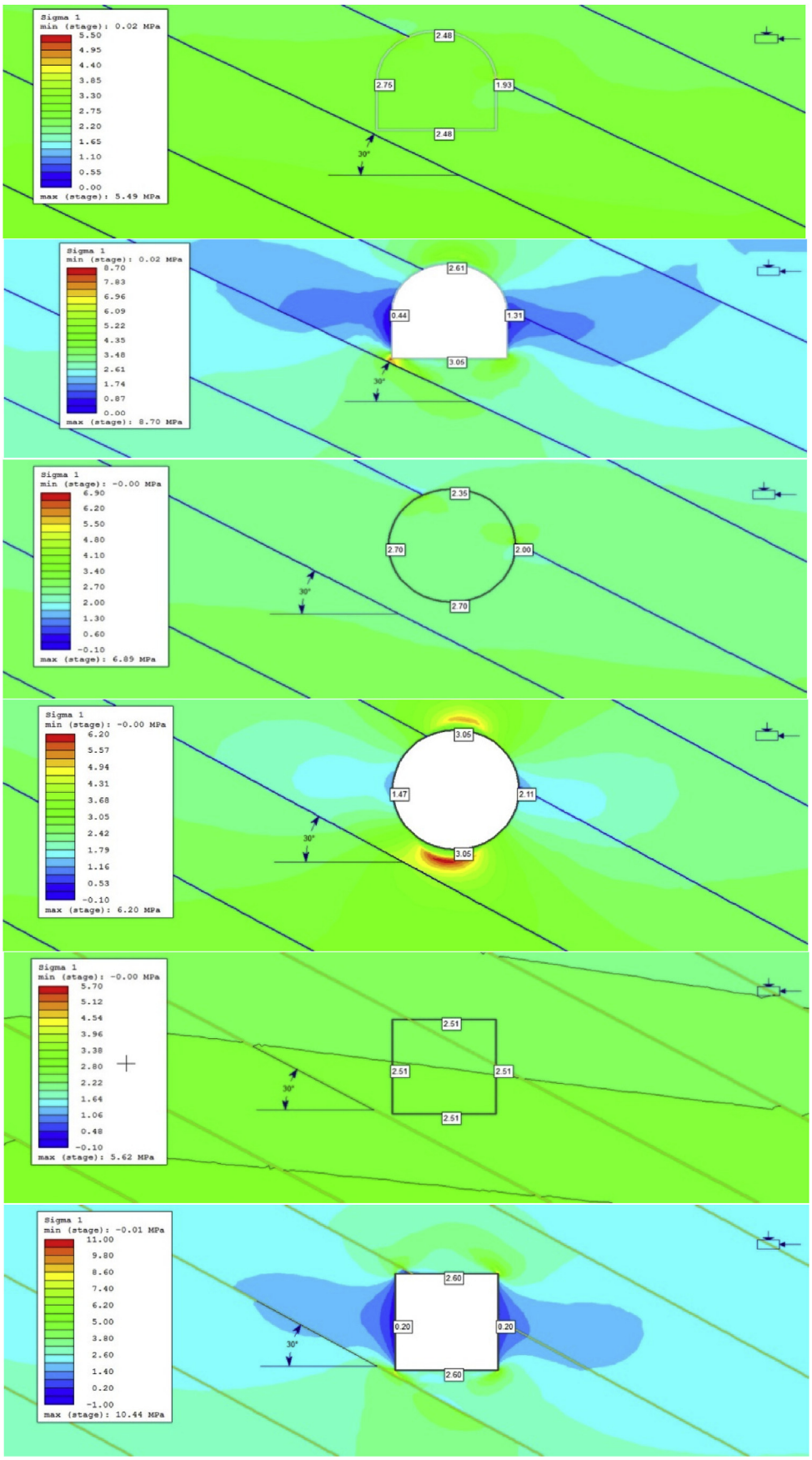

Fig. 15. Contours of pre- and post-excavating boundary stresses of different tunnel shapes.

Table 5
Pre-, post- and induced-stresses in various tunnel shapes when joints included in the rock mass.

Tunnel shape	Pre-excavating boundary stress, σ_0 MPa				Post-excavating boundary stress, σ_1 MPa				Estimated induced-stress, MPa ($\sigma_1 - \sigma_0$)			
	Roof (#1)	Left wall (#2)	Right wall (#3)	Floor (#4)	Roof (#1)	Left wall (#2)	Right wall (#3)	Floor (#4)	Roof (#1)	Left wall (#2)	Right wall (#3)	Floor (#4)
Circular	2.35	2.70	2.0	2.70	3.05	1.47	2.11	3.05	0.70	−1.23	0.11	0.35
Horseshoe	2.48	2.75	1.93	2.48	2.61	0.44	1.31	3.05	0.13	−2.31	−0.62	0.57
Square	2.51	2.51	2.51	2.51	2.60	0.20	0.20	2.60	0.09	−2.31	−2.31	0.09

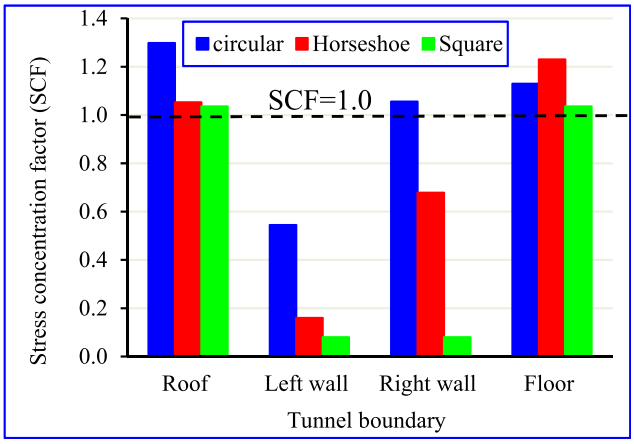

Fig. 16. Stress concentration values around the boundary of different tunnel shapes.

4.1.3. Extent of yielding zones

Fig. 13 shows the spread of failure zones into rock mass around tunnel boundaries. It can be shown that rock mass fails only around a tunnel's roof and floor. Also, it is noticeable that yielding occurs around curved surfaces (e.g. in circular tunnels and the roof of horseshoe tunnels). However, failure occurs in of "cone-shaped" form around flat or right-angled surfaces (e.g. in square tunnels and the floor of horseshoe tunnels). The maximum extent of yielding zones occurs in the roof of square tunnels, this being 0.873 m, and in the floor of horseshoe tunnels, this being 1.128 m. By comparing the extent of yielding zones with the minimum anchorage length of rock support (0.30 m) it can be observed that the performance of the tunnels is satisfactory. Alternatively, the performance of the tunnel will be unstable or unsatisfactory if the extent of yielding exceeds 1.50 m for a rockbolt of 1.80 m in length, as insufficient anchorage length will be left < 0.30 m.

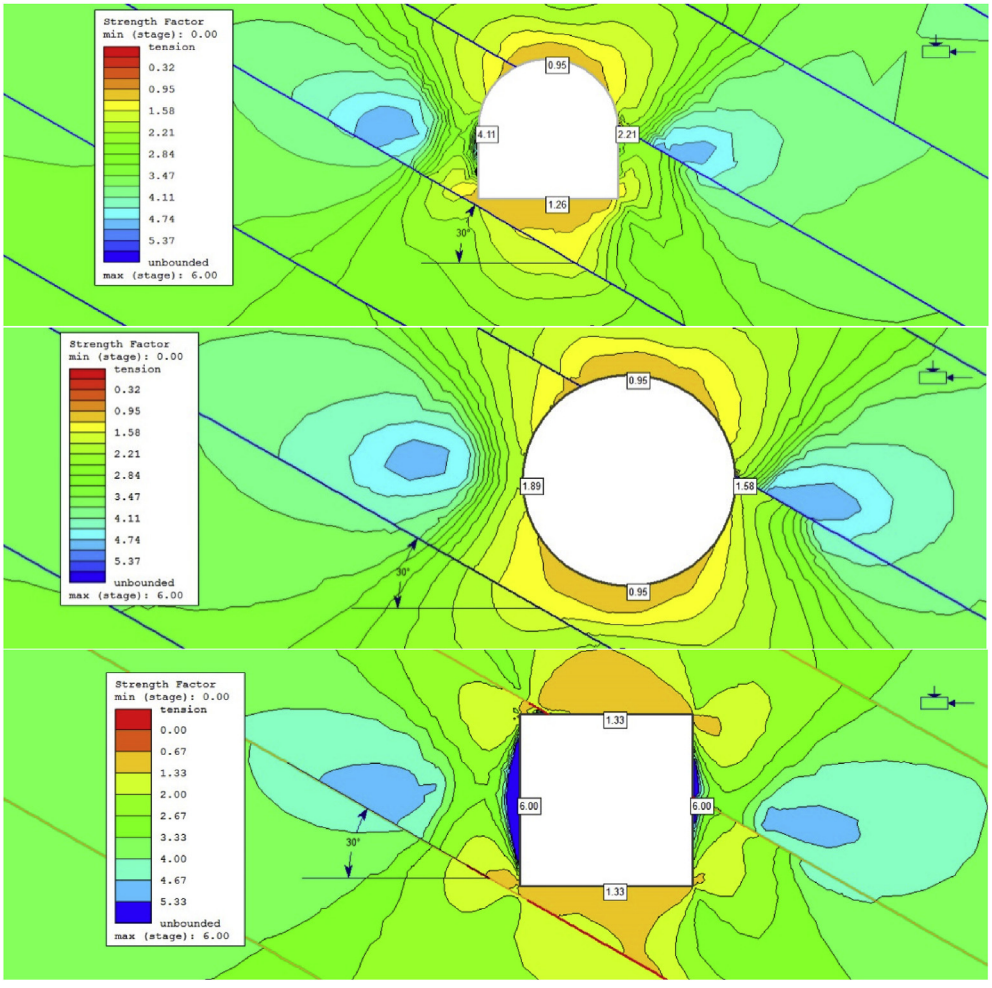

Fig. 17. Strength contours of rock mass around the boundary of different tunnel shapes.

4.2. Case II– rock joints included

A parallel set of a joint network with a dip angle of 30° is included in the model in order to study their effect on tunnel performance. The geomechanical properties of rock joints used in this analysis are listed in Table 4. Fig. 14 shows the model geometry of the horseshoe tunnel, including joints.

The analysis has been carried out for the three tunnel shapes (circular, horseshoe and square). The results will be presented and discussed in terms of the state of stress-displacements in the rock mass surrounding a tunnel's boundary. In addition, normal and shear stresses and shear displacement along rock joints will be introduced and discussed.

4.2.1. Induced-stress

The contours of pre- and post-excavating boundary stresses, after including joints in the rock mass matrix, are plotted as shown in Fig. 15. Consequently, the induced-stresses are estimated as listed in Table 5 and depicted in Fig. 16 for different tunnel shapes.

The results show that the estimated induced-stresses, when rock joints are included, are higher than those obtained without including joints. For instance, the maximum induced-stress (compressive) is found around the roof of a circular tunnel (about 0.70 MPa when including rock joints compared to 0.25 MPa without including joints). Whereas, the minimum induced-stress (tensile) is found around the sidewalls of a square tunnel (−2.88 MPa when no joints are included compared to −2.31 MPa when joints are included). Therefore, the difference in the induced-stresses is attributed to the presence of rock joints.

4.2.2. Stress concentration factor (SCF)

Fig. 16 shows the stress distribution in the rock mass after creating a tunnel opening represented by the strength concentration factor, *SCF*. It can be shown that the locations and magnitudes of *SCF* are different when compared with those obtained when rock joints are not present. For instance, the highest *SCF* is 1.30 (around the roof of circular tunnel) compared with 1.11 (around the floor of the square tunnel). Also, another difference is that, all values of stress concentrations (*SCF*) are positive (when joints are included) compared to some negative *SCF* values which occur around the sidewalls of a square tunnel (when joints are not present).

For example, the *SCF* is +0.08 when joints are included compared to −0.05 when joints are not present in the sidewalls of the square tunnel.

4.2.3. Strength factor (SF)

Fig. 17 depicts the strength contours of rock mass (represented by strength factor or factor of safety) around the boundary of different tunnel shapes. It can be shown that the strength of rock mass deteriorates around the roof and the floor of circular tunnels and around the roof of horseshoe tunnels (*SF* < 1.0). In addition, there is discontinuity in the strength contours of rock mass when they are intersected by rock joints.

4.2.4. Deformation/convergence

In this section, only horizontal and vertical displacements are presented, compared and discussed in terms of wall convergence ratio (*WCR*), roof sag ratio (*RSR*) and floor heave ratio (*FHR*).

4.2.4.1. Wall convergence ratio (WCR). Fig. 18 shows the estimated convergence ratio in the tunnel's sidewalls at various lateral displacements from the key points (i.e. points #2 & #3) and for different tunnel shapes. It can be shown that the tunnel's sidewalls tend to move towards the entire of the tunnel after an opening has been excavated. In addition, maximum wall convergence occurs in the sidewalls of the square tunnel when rock joints are included (wall convergence ratios *WCRs* are −0.0138% and 0.0048% when joints are included compared to ∓0.009% when joints are not present). Alternatively, when a rock mass matrix comprises of rock joints along with intact rock, the horizontal displacement in the right wall of the square tunnel (point #3) increases by 1.5-times and in the left wall (point #2) is almost reduced by 50%. However, the serviceability of all tunnels (circular, horseshoe and square) is still satisfactory (*WCR* < 2%).

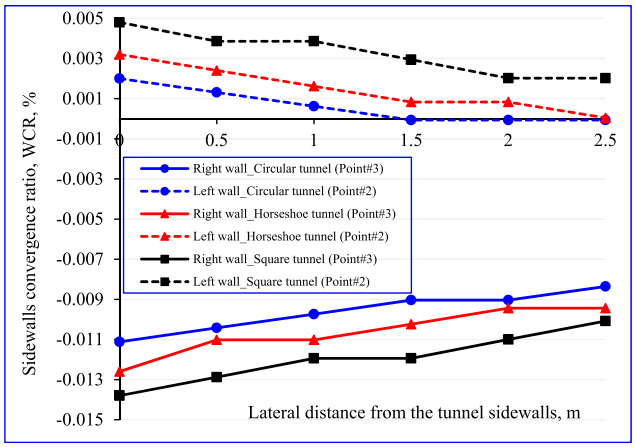

Fig. 18. Side walls convergence ratio for different tunnel shapes when rock joints are present in the rock mass matrix.

4.2.5. Ratio of roof sag (RSR) and floor heave (FHR)

Fig. 19 depicts the roof sag and the floor heave ratio that occur in a tunnel's roof (point #1) and floor (point #4) respectively when rock joints are included in the rock mass matrix. The results show that, the *RSR* and *FHR* values are higher than those obtained when rock joints are not present. For instance, the maximum roof sag ratio is −0.0155% (compared to −0.0044%), and the maximum floor heave ratio is −0.0074% (compared to +0.00406%) occur in the square tunnel when joints are included. Moreover, the results show that, the tunnel's floor tends to move downwards (negative values) when rock joints are included compared to its movement upwards when there are no joints are present. Therefore, the state of stress displacement along rock joints is introduced in the last section.

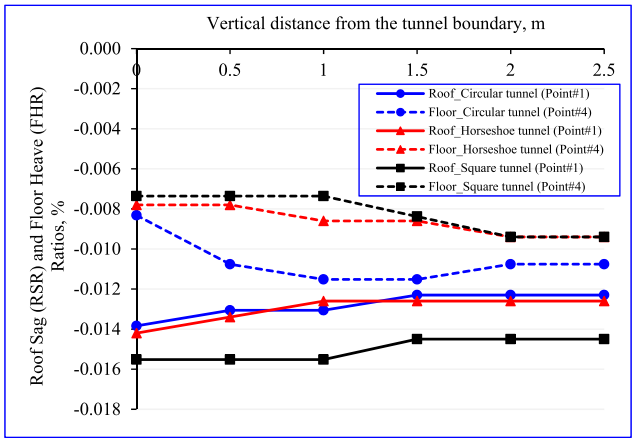

Fig. 19. Roof sag and floor heave ratio for different tunnel shapes estimated at various vertical distances measured from a tunnel's boundary (key points #1 & #4).

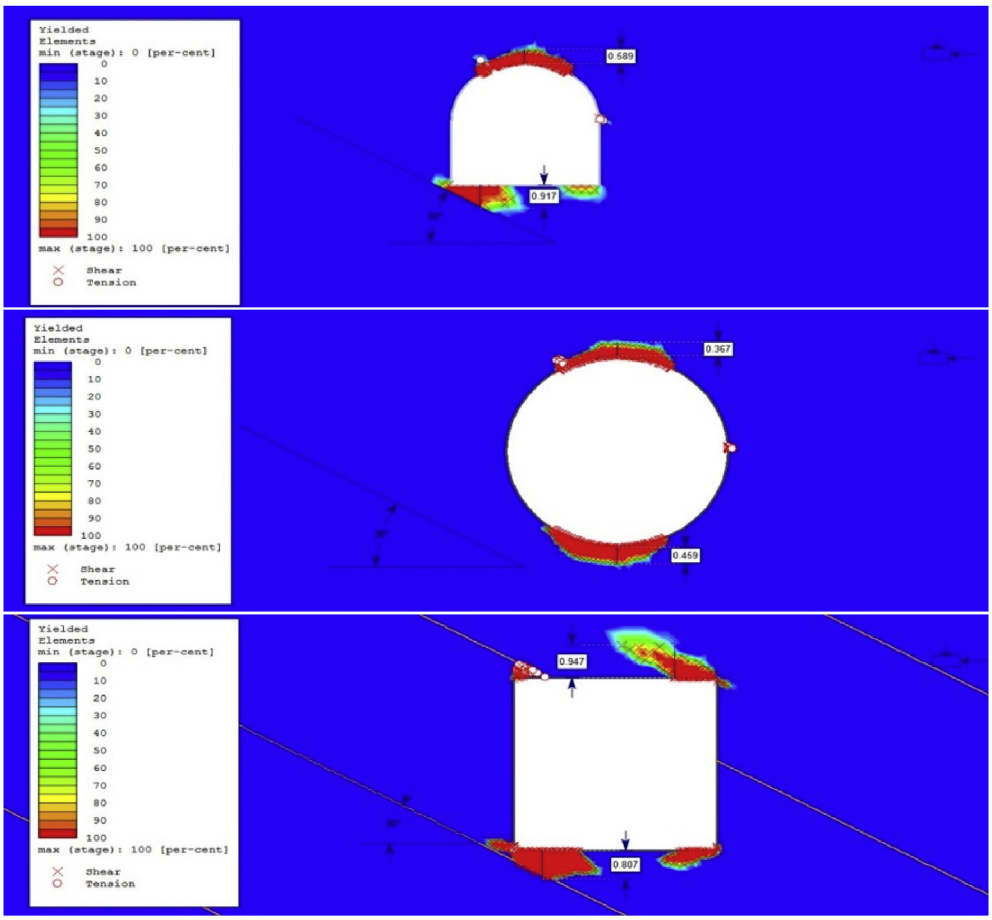

Fig. 20. Extent of failure zones around the boundary of different tunnel shapes when joints are present in the rock mass.

4.2.6. Stress concentration factor (SCF)

Fig. 5 depicts the locations of stress concentration around the boundary of different tunnel shapes. It can be shown that compressive stresses are concentrated around the roof and the floor of a circular tunnel (e.g. $SCF > 1.0$). Whereas, tensile stresses are concentrated around the sidewalls of a square tunnel (e.g. negative or $SCF < 0.0$).

4.2.7. Strength factor (SF)

The *SF* is defined as (Eq. (3)) the ratio of the lab unconfined strength of intact rock (*UCS*) to the induced-stress. The performance of the tunnel becomes satisfactory if $SF > 1$. Fig. 6 shows the contours of rock strength around a tunnel's boundary. It can be shown that the roof of a horseshoe tunnel, and the roof and the floor of a circular tunnel are unstable ($SF < 1.0$).

4.2.8. Extent of yielding zones

Fig. 20 presents the spread of the failure (plastic) zones around the boundary of different tunnel shapes. It can be shown that the rock mass fails around the sharp corners of square tunnels, along the roof and the floor of circular tunnels and along the floor of horseshoe tunnels. The shapes of yielding zones and their locations are different when compared with those that occurred when rock joints were absent. The maximum extents of the yielding zones are 0.947 m (in the roof's right corner in square tunnels) and 0.917 m (in the floor's left corner in horseshoe tunnels). However, these lengths are still beyond the maximum permissible extent of yielding zones (< 1.50 m). Therefore, the tunnel's performance is considered satisfactory.

4.2.9. Stresses and displacement along joints

Fig. 21 shows the distribution of normal stresses along rock joints for different tunnel shapes. The results show that high normal stresses are concentrated along rock joints at the sidewalls of a tunnel's boundary. Monitoring the maximum normal stresses along rock joints at a distance of ∓ 2.5 m from the tunnel centre (as the dimensions of the tunnel are 5×5 m), see Fig. 22. It is clear that the normal stresses around the left and the right walls of the square tunnel are 1.52 MPa and 1.78 MPa respectively. For the horseshoe

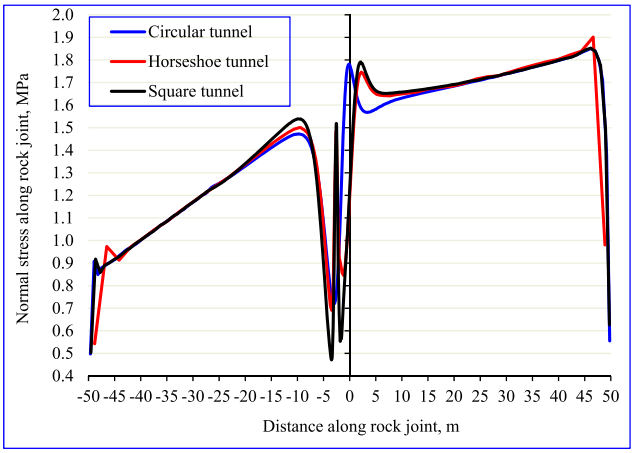

Fig. 21. Normal stresses along yielded rock joints for different tunnel shapes.

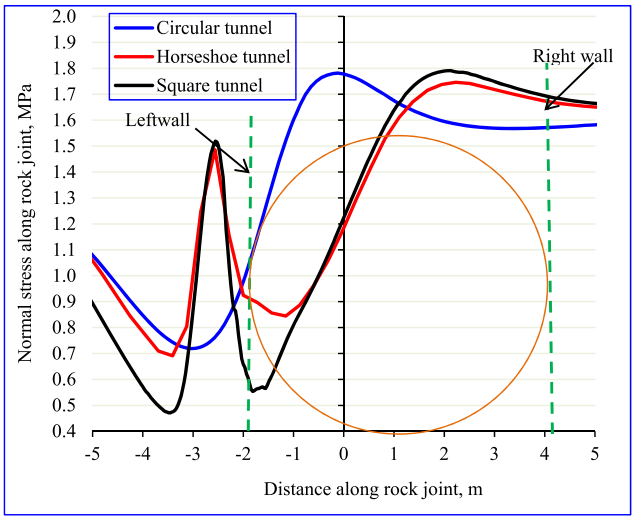

Fig. 22. Zoom in for the normal stresses along joints at distance ranges of ∓2.5 m from the centre of the tunnel.

tunnel, the normal stresses along joints around the left and the right walls are 1.49 MPa and 1.74 MPa respectively. Whereas, the normal stresses along rock joints around the left and the right walls of the circular tunnel are 0.78 MPa and 1.58 MPa respectively.

The shear stresses along rock joints for different tunnel shapes are shown in Fig. 23. The minimum and maximum shear stresses along rock joints are approximately −0.45 MPa and 1.41 MPa (square tunnel). The shear displacements along rock joints in various tunnel shapes are depicted in Fig. 24. The minimum and the maximum shear displacements which occur along rock joints are −0.0313 mm and 0.3078 mm respectively for the square tunnel.

5. Conclusion

This paper presents the results of parametric stability analysis to investigate the effect of some crucial parameters on the performance of shallow tunnels. In this study, only two factors have been examined, namely tunnel shape (circular, horseshoe and square) and the presence of rock joints (parallel set of joint networks that dip by 30°) in the rock mass matrix (slate and limestone rock mass).

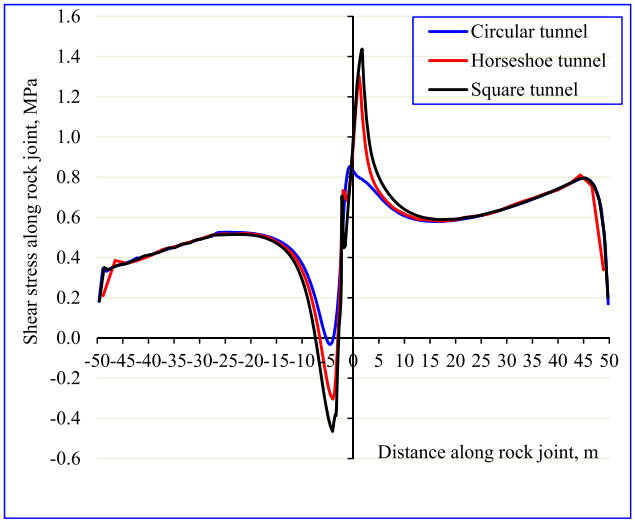

Fig. 23. Shear stress distribution along yielded rock joints for different tunnel shapes.

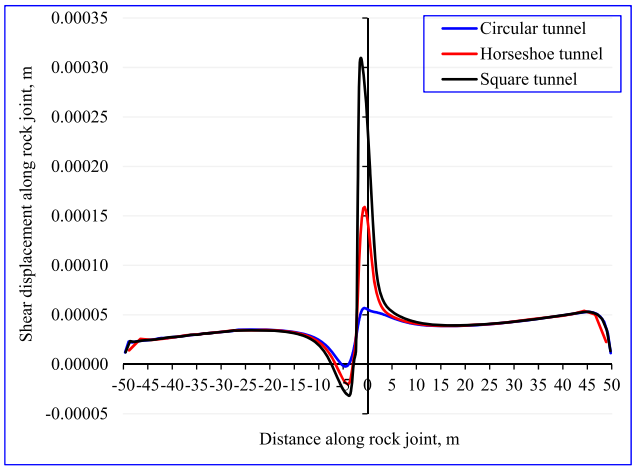

Fig. 24. Shear displacement along yielded rock joints at various tunnel shapes.

A two-dimensional elasto-plastic finite element, RS^{2D}, code was employed with the Mohr-Coulomb failure criterion. The tunnel is situated at 50 m below the ground surface and excavated in limestone rock mass. The behaviour of the tunnel opening is monitored in terms of the state of stress-displacement using four reference points that are assigned in the tunnel's perimeter. Consequently, several performance evaluation criteria have been used to assess the serviceability of the tunnel opening (induced-stress, stress concentration factor, strength factor, sidewalls convergence ratio, roof sag ratio, floor heave ratio and the extent of yielding zones in the rock mass surrounding the tunnel opening).

In addition, normal and shear stresses and shear displacement along rock joints were investigated. The results reveal that the stability of a tunnel significantly deteriorates post-excavation (particularly in a square tunnel). In addition, the performance of the tunnel prominently deteriorates when rock joints are present along with the rock mass matrix. Moreover, the continuity of the strength contours of rock mass around the tunnel boundary is not persistent when they are intersected by rock joints. Maximum deformations and stresses are concentrated around the tunnel boundary (at a distance of 0.0 m from the tunnel boundary).

Furthermore, the results show that the normal stress along rock joints is maximized at the tunnel boundary; however, it sharply dropped when joints intersect the tunnel. In addition, the direction of shear stress along rock joints is reversed when joints pass or intersect the tunnel (slip occurrence). Therefore, inward shear displacement is resulted in along rock joints. However, based on the chosen thresholds of the failure evaluation criteria, the performance of all tunnels is still satisfactory with and without rock joints and with various tunnel shapes.

Recommendations

Other parameters can be included into the sensitivity analysis, such as: joins geometrical properties (stiffness, roughness, friction, dip/dip directions, joint spacing, etc.), in-situ stress ratio (horizontal-to-vertical stress ratio), depth of the tunnel below the surface, size of the opening, rock mass properties (cohesion, friction, deformation modulus, etc.) to investigate the most crucial parameter(s) influencing tunnel stability.

Conflict of interest

None declared.

Ethical statement

Authors state that the research was conducted according to ethical standards.

Funding body

None.

Acknowledgments

The authors acknowledge the support of Rocscience Inc. for getting a free two-week RS2D software. The authors are grateful for their support. For more information about RS2D software, the reader is directed to the following link: https://www.rocscience.com/rocscience/products/rs2

Nomenclature

$\sigma_v = \gamma_{avg} \times Z$	Overburden or vertical in-situ stress
$\sigma_h = K \times \sigma_v$	Lateral in-situ stress
K	Horizontal-to-vertical in-situ stress ratio
z	Depth below surface
σ_t	Tensile strength of rock mass
γ	Unit weight of rock mass
υ	Poisson's ratio
UCS	Lab unconfined compressive strength of intact rock
E	Young's Modulus of rock mass
C	Cohesion of rock mass
$\varnothing$	Internal friction angle of rock mass
ψ	Dilation angle of rock mass ($\psi = \phi/4$)

References

Abdellah, W. R. E. (2015). Numerical modelling stability analyses of haulage drift in deep underground mines. *Journal of Engineering Science, 43*(1), 71–81.

Abdellah, W., Mitri, H. S., Thibodeau, D., & Moreau-Verlaan, L. (2012). Stochastic evaluation of haulage drift unsatisfactory performance using random Monte-Carlo simulation. *International Journal of Mining and Mineral Engineering, 4*(1), 63–87. https://doi.org/10.1504/IJMME.2012.048000.

Barton, N. R. (1972). A Model study of rock-joint deformation. *International Journal of Rock Mechanics and Mining Science & Geomechanics Abstracts, 9*(5), 579–582. https://doi.org/10.1016/0148-9062(72)90010-1.

Berisavljević, Z., Berisavljević, D., Čebašek, V., & Rakić, D. (2015). Slope stability analyses using limit equilibrium and strength reduction methods. *Građevinar, 67*(10), 975–983. https://doi.org/10.14256/JCE.1030.2014.

Brady, B. H. G. (1977). An analysis of rock behaviour in an experimental stoping block at the Mount Isa Mine, Queensland, Australia. *International Journal of Rock Mechanics and Mining Science & Geomechanics Abstracts, 14*(2), 59–66. https://doi.org/10.1016/0148-9062(77)90197-8.

Brady, B., & Lorig, L. (1988). Analysis of rock reinforcement using finite difference methods. *Computers and Geotechnics, 5*(2), 123–149. https://doi.org/10.1016/0266-352X(88)90042-0.

Eberhardt, E. (2001). Numerical modelling of three-dimension stress rotation ahead of an advancing tunnel face. *International Journal of Rock Mechanics and Mining Sciences, 38*(4), 499–518. https://doi.org/10.1016/S1365-1609(01)00017-X.

Elshamy, E. A., Attia, G., Fawzy, H., & Abdel Hafez, K. (2013). Behavior of different shapes of twin tunnels in soft clay soil. *International Journal of Engineering and Innovative Technology, 2*(7), 297–302.

Ghorbani, K., Zahedi, M., & Asaadi, A. (2015). Effects of statistical distribution of joint trace length on the stability of tunnel excavated in jointed rock mass. *International Journal of Mining and Geological Engineering, 49*(2), 289–296.

Goodman, R. E., Heuze, F. E., & Bureau, G. J. (1972). On modeling techniques for the study of tunnels in jointed rock. In *Conf. Proc. of the 14th U.S. Symposium on rock mechanics (USRMS), 11–14 June, University Park, Pennsylvania USA*. https://www.onepetro.org/conference-paper/ARMA-72-0441.

Goodman, R. E., & Shi, G. H. (1985). *Block theory and its application to rock engineering*. Englewood Cliffs, NJ: Prentice-Hall, Inc.

Hao, Y. H., & Azzam, R. (2005). The plastic zones and displacements around underground openings in rock masses containing a fault. *Tunnelling and Underground Space Technology, 20*(1), 49–61. https://doi.org/10.1016/j.tust.2004.05.003.

Jeon, S., Kim, J., Seo, Y., & Hong, Ch (2004). Effect of a fault and weak plane on the stability of a tunnel in rock – a scaled model test and numerical analysis. *International Journal of Rock Mechanics and Mining Sciences, 41*(1), 658–663. https://doi.org/10.1016/j.ijrmms.2004.03.115.

Jethwa, J. L., Dube, A. K., Singh, B., & Singh, B. (1984). Squeezing problems in Indian tunnels. In *Conf. Proc. of the first international conference on case histories in geotechnical engineering*. USA: Missouri University of Science and Technology. Retrieved January 2018 from:http://scholarsmine.mst.edu/icchge/1icchge/1icchge-theme7/7.

Jiang, Y., Tanabashi, Y., Li, B., & Xiao, J. (2006). Influence of geometrical distribution of rock joints on deformational behavior of underground opening. *Tunnelling and Underground Space Technology, 21*(5), 485–491. https://doi.org/10.1016/j.tust.2005.10.004.

Jia, P., & Tang, C. A. (2008). Numerical study on failure mechanism of tunnel in jointed rock mass. *Tunnelling and Underground Space Technology, 23*(5), 500–507. https://doi.org/10.1016/j.tust.2007.09.001.

Kirsch, G. (1898). Die theorie der elastizitat und die bedürfnisse der festigkcitslchre. *Veit Ver Deut Ing, 42*, 797–807.

Kulatilake, P. H. S. W., Qiong, W., Zhengxing, Y., & Fuxing, J. (2013). Investigation of stability of a tunnel in a deep coal mine in China. *International Journal of Mining Science and Technology, 23*(4), 579–589. https://doi.org/10.1016/j.ijmst.2013.07.018.

Ladanyi, B. (1974). Use of the long-term strength concept in the determination of ground pressure on tunnel linings. In *Conf. Proc. of the advances in rock mechanics, proceedings of the third congress, international society of rock mechanics, Denver*. National Academy of Sciences.

Madkour, H. (2012). Parametric analysis of tunnel behavior in jointed rock. *Ain Shams Engineering Journal, 3*(2), 97–103. https://doi.org/10.1016/j.asej.2012.01.002.

Maleki, M. R., Mahyar, M., & Meshkabadi, K. (2011). Design of overall slope angle and analysis of rock slope stability of chadormalu mine using empirical and numerical methods. *Engineering, 3*, 965–971. https://doi.org/10.4236/eng.2011.39119.

Martin, C. D., Kaiser, P. K., & McCreath, D. R. (1999). Hoek-Brown parameters for predicting the depth of brittle failure around tunnels. *Canadian Geotechnical Journal, 36*, 136–151.

Mitri, H. S. (2007). Assessment of horizontal pillar burst in deep hard rock mines. *International Journal of Risk Assessment and Management, 7*(5), 695–707. https://doi.org/10.1504/IJRAM.2007.014094.

Panjia, M., Koohsari, H., Adampira, M., Alielahi, H., & Marnani, J. A. (2016). Stability analysis of shallow tunnels subjected to eccentric loads by a boundary element method. *Journal of Rock Mechanics and Geotechnical Engineering, 8*(4), 480–488. https://doi.org/10.1016/j.jrmge.2016.01.006.

Piyal, W. P. L., & Konietzky, H. H. (2016). *Geometrical properties of rock joints and their effects on rock mechanical behaviour*. Retrieved 19 December 2016 from: https://tu-freiberg.de/fakult3/gt/feme/e-book/13_Geometrical_properties_of_rock_joints_and_their_effects_on_rock_mechanical_behaviour.pdf.

Raju, G. D. (2013). *Methodology for the design of dynamic rock supports in burst prone ground*. Ph.D. Thesis. Montreal, Canada: McGill University.. Retrieved August 2013 from: http://digitool.library.mcgill.ca/webclient/StreamGate?folder_id=0&dvs=1517032365593-227.

Saini, G. S., Dube, A. K., & Singh, B. (1989). Severe tunneling problems in young Himalayan rocks for deep underground opening. In *Conf. Proc. of the ISRM international symposium. Pau, France*. Retrieved January 2018 from:https://search.spe.org/i2kweb/SPE/doc/onepetro:0A09479E/.

Sheorey, P. R. (1997). *Empirical rock failure criteria*. Taylor & Francis.

Soren, K., Budi, G., & Sen, P. (2014). Stability analysis of open pit slope by finite difference method. *International Journal of Renewable Energy Technology, 3*(5), 326–334.

Yeung, M. R., & Leong, L. L. (1997). Effects of joint attributes on tunnel stability. *International Journal of Rock Mechanics and Mining Sciences, 34*(3–4), 348. https://doi.org/10.1016/S1365-1609(97)00286-4. e341–348.e318.

Zhang, Y., & Mitri, H. S. (2008). Elastoplastic stability analysis of mine haulage drift in the vicinity of mined stopes. *International Journal of Rock Mechanics and Mining Sciences, 45*(4), 574–593. https://doi.org/10.1016/j.ijrmms.2007.07.020.